Journal of Applied Electrochemistry **31**: 1213–1220, 2001.

The use of a segmented tool for the analysis of electrochemical machining

A.R. MOUNT[1]*, P.S. HOWARTH[1] and D. CLIFTON[2]
[1]*Department of Chemistry;* [2]*Department of Mechanical Engineering, University of Edinburgh, King's Buildings, West Mains Road, Edinburgh EH9 3JJ, UK*
*(*author for correspondence, e-mail: a.mount@ed.ac.uk)*

Received 9 May 2001; accepted in revised form 14 August 2001

Key words: characterisation, current analysis, electrochemical machining, segmented tool

Abstract

A planar workpiece/planar segmented tool experimental configuration has been used to collect current–time data for the electrochemical machining (ECM) of Inconel 718 (In718) and stainless steel (SS316). As with previous measurements, theoretical analysis of the chronoamperometric data has been used to obtain values for the characteristic parameters of ECM under characteristic machining conditions, but the segmented tool allows this for each segment. These parameters are the valency, n, and k, from which the minimum voltage required to initiate machining, V_0, and the electrolyte conductivity, κ can be obtained. The variation of n, V_0 and κ between segments enables ECM conditions along the flow path length to be probed. Measurements on In718 in nitrate electrolyte have shown a small increase in electrolyte conductivity along the flow path. Tool segments which overlap the workpiece ends have been employed to measure edge effects in the ECM process; no significant edge effects were found when machining In718 in nitrate. The temporal and spatial dependences of a change in valency previously observed during the machining of SS316 have also been studied for the first time. Regions of low valency ($n = 2.1$) dissolution (downstream) and high valency (upstream, $n = 3.0$) dissolution were observed, with an intermediate region with monotonically decreasing valency where $3.0 > n > 2.1$.

1. Introduction

Increasing demand for high strength, low-weight, metallic and intermetallic alloys has led to an increasing requirement for metal cutting and forming processes able to cope effectively with such materials. Electrochemical machining (ECM), whereby metal is removed by the electrochemical dissolution of a workpiece material, offers many potential advantages over traditional methods of machining, as ECM is able to machine a material irrespective of hardness and is able to produce complex shapes at high metal removal rates. A high quality surface is produced without residual stresses or surface damage to the microstructure [1–5]. ECM is carried out by passing an electric current of up to 100 A cm^{-2} through an electrolyte flowing in the gap between an electrode tool (biased as the cathode) and workpiece (biased as the anode). As dissolution of the workpiece material occurs the tool electrode is advanced, at a controlled rate, to maintain removal of material.

Previous work [6] has demonstrated how chronoamperometric measurements of ECM using a planar workpiece/planar tool configuration with a constant tool feed rate can be analysed to obtain direct measurements of chemical parameters such as the electrolyte conductivity, the valency and the surface overpotential [7–11]. These are the crucial parameters for process simulation [12, 13] and tool design [14, 15] in ECM and they can also be used to give insight into the chemical dissolution processes occurring. Such measurements take no account of the variation of the nature and concentration of the ions in the flowing electrolyte across the workpiece surface during ECM. Upstream of the workpiece the electrolyte composition is the same as that in the electrolyte reservoir. However, as electrolyte flows across the workpiece surface, soluble metal ions are produced and electrolyte ions consumed, the temperature increases due to resistive heating [16] and the void fraction may increase due to gaseous products [17, 18]. These may lead to a progressive change in electrolyte conductivity and composition, which could induce variation in the ECM parameters with flow path length. This paper presents the analysis of flow path variation using a segmented tool system. A segmented tool (or sectional cathode) [19] has previously been reported for use in machining of large surface areas, with each segment under independent voltage control. However, this novel system has been developed to allow theoretical analysis of current transient data specifically to obtain ECM parameters along the flow path length.

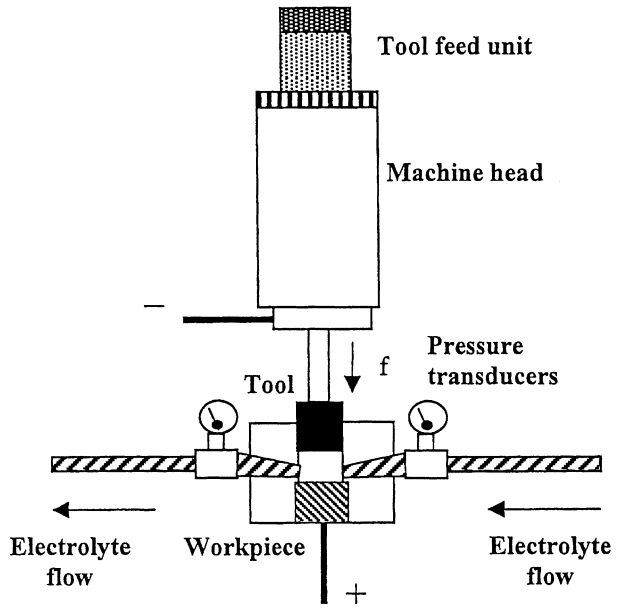

Fig. 1. The experimental configuration for the ECM machining experiments.

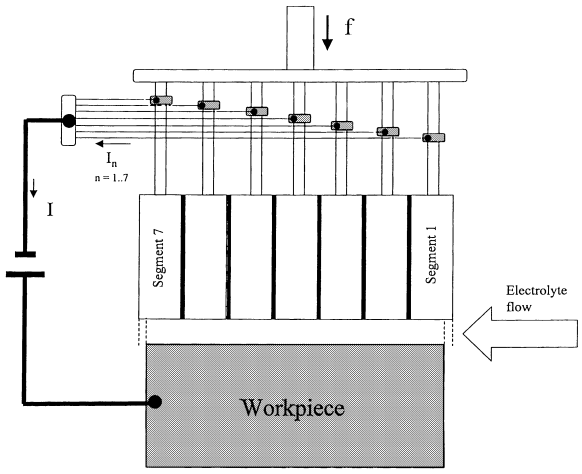

Fig. 2. The experimental configuration of the segmented tool system.

2. Experimental

The experimental setup for these measurements is as given previously ([6] and Figure 1). This consisted of a Transtec electrochemical machine, with an RDOA regulating transformer (Bonar Brentford Electric), a 600 A transformer (Goodyear), a Hydracell D25 electrolyte pump (Wanner Engineering Inc.), a type FT 13 (Platon Instrumentation) flow sensor and type HT (RS Components) current transducers. The data were collected using a PC with Intelligent Instruments (Burr–Brown) in house data logging system. A reservoir of 60 l of electrolyte was used, kept at 30 °C. As with the previous paper [6] the system under consideration is a planar tool moving at a constant feed rate, f, towards a planar parallel alloy workpiece, each of metallic area $A = 4.80\ \text{cm}^2$. However, in this work the tool was divided into seven separate coplanar electrodes (or segments) with relatively narrow insulation separating them (Figure 2). These were numbered segments 1–7 from upstream to downstream in the electrolyte flow as shown. Seven current transducers were used to detect the current for each segment and one transducer was used to measure the total combined current from all segments. All transducers were calibrated and the total current was consistently found to be equal to the sum of the segmented currents within experimental error (~0.5%). In contrast to previous studies [6], it should be noted that due to the introduction of insulation separating each segment, the overall length of the segmented tool in this setup was greater than the workpiece and hence segments 1 and 7 on the segmented tool overlapped the workpiece at each end. This had the advantage of enabling the measurement of edge effects, which have been suggested as being important in ECM [20].

The two electrolyte systems employed were a 2.56 mol dm^{-3} (15.0% w/v) aqueous solution of sodium chloride and a 2.56 mol dm^{-3} (21.7% w/v) aqueous solution of sodium nitrate (Anderson, Gibb and Wilson) and the workpiece alloys were SS316 and In718 (Haynes International Inc.). The certified compositions of these alloys are given in Table 1.

The initial electrode gap was measured by casting, using a polyether impression material (EPSE Permadyne). This initial gap was 0.80 mm for these experiments unless otherwise stated. A constant voltage, V, was applied between the workpiece and the tool. The electrolyte flow rate and feed rate, f, were also held constant throughout at 20.0 $\text{dm}^3\ \text{min}^{-1}$ and 1.00 mm min^{-1} respectively unless otherwise stated. Under these relatively high flow conditions, assuming that the movement of each electron in the external circuit results in the production of one anion and one cation in the electrolyte at the tool and the workpiece respectively and an upper limit for I_∞ of 350 A for these experiments, this corresponds to a maximum increase in ion concentration of 2.2×10^{-2} mol dm^{-3} during machining. From this the calculated change in electrolyte concentration is of the order of 1%. These conditions therefore ensure that the approximation of constant overall electrolyte concentration along the flow path length is reasonable.

Table 1. Composition in weight percent of In718 and SS316 alloys

Alloy	C	Fe	S	Al	P	Mn	Co	Cr	Cu	Mo	Ni	Si	Ti
SS316	0.12[a]	70.09	0.045[a]	–	0.045[a]	2.00[a]	–	17.00	–	2.50	8.00	0.02[b]	–
In718	0.05	18.45	–	0.48	–	0.22	0.17	18.16	0.02	2.96	53.32	0.10	1.02

[a] Maximum value; [b] Minimum value.

However, at lower flow rates, this approximation is less valid.

Fitting of the current–time transients I_2–I_6 was achieved by iteratively fitting the results to Equation (9), using the SigmaPlot plotting program (Jandel Scientific).

3. Results and discussion

3.1. *Calibration of the segmented tool apparatus*

The first test of the planar segmented tool/planar workpiece system was to compare and contrast its response to that of the planar single tool/planar workpiece. Previous studies [6] have shown that the planar single tool/planar workpiece configuration can successfully be used to obtain and analyse current–time data for the ECM of In718 in nitrate electrolyte at relatively high electrolyte flow rates and extract independent values for the machining parameters κ, V_0 and n. This suggests there is little significant variation in these ECM dissolution parameters across the workpiece surface, which greatly simplifies analysis for calibration. Theoretical analysis assumed the current to be governed by migration (an essential assumption for stable machining). Furthermore, since the tool and workpiece were parallel, of equal dimensions (area A) and separated vertically in this system, the field lines between the two electrodes could be assumed to be normal and vertical between the two electrodes (Figure 3a). The conductivity, κ, could be assumed to be constant [6] as the electrolyte flow rate was sufficient to minimise the change in concentration due to the build up of machining products and/or the loss of ions from the electrolyte, the temperature increase along the path length and the void fraction of evolved gases in the electrolyte, all of which can affect the conductivity. In this case, if the gap between the electrodes is z, the current across the electrolyte, I, is given by:

$$I = \frac{\kappa(V - V_0)A}{z} \tag{1}$$

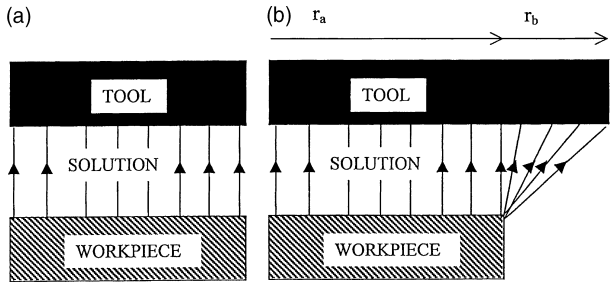

Fig. 3. Migration field lines (a) for the planar single tool system and for each of the segments 2–6 in the segmented tool system (b) for each of the end segments 1 and 7 in the segmented tool system. The distances corresponding to r_a and r_b are shown for segments 1 and 7. For these experiments $r_a = 4.69$ mm, $r_b = 1.31$ mm and hence $r_n = r_a + r_b = 6.00$ mm.

where V is the applied voltage, V_0 is that portion of the voltage required at the two electrodes to drive the electrode reactions (*vide infra*) and κ is the conductivity of the electrolyte. Assuming that all current leads to electrode dissolution (100% dissolution efficiency), this current is also the dissolution current of the workpiece, and therefore

$$I = \left[\frac{nFA\rho}{M}\right]\frac{dy}{dt} \tag{2}$$

where n is the average number of electrons required to be removed to dissolve each atom (the 'valency'), F is Faraday's constant (96 485 C mol^{-1}), ρ is the density of the workpiece material, dy/dt is the thickness of workpiece removed per unit time and M is the average molecular weight (the mass of 1 mol) of the workpiece material. It has been reported that efficiencies below 100% are obtained in some cases at low flow rates [16, 21–23], under which conditions n should be replaced by the more general term n/e in Equation (2), where e is the efficiency. However, efficiency has been observed to increase with flow rate and approach 100% ($e = 1$) at flow rates significantly lower than that employed throughout this work [21]. Furthermore, the measured invariance of n with current and interelectrode distance in this and previous work [6] (as demonstrated by the closeness of theoretical fits to the data) and the invariance of n with segment number (*vide supra*) all indicate a constant value of e, which would not be expected for efficiencies significantly below 100%.

The change in the interelectrode distance, z, is given by

$$\frac{dz}{dt} = \frac{dy}{dt} - f \tag{3}$$

and hence, combining Equations (1)–(3)

$$\frac{dz}{dt} = \frac{k}{z} - f \tag{4}$$

where

$$k = \left[\frac{\kappa(V - V_0)M}{nF\rho}\right] \tag{5}$$

Now at the equilibrium current, I_∞, (I when $t \to \infty$), when a steady-state current has been reached, z remains constant at z_∞ and $dz/dt = 0$; hence $f = k/z_\infty$,

$$I_\infty = \left[\frac{nFA\rho}{M}\right]f \tag{6}$$

and

$$\frac{dz}{dt} = k\left[\frac{1}{z} - \frac{1}{z_\infty}\right] \tag{7}$$

Equation (7) can be integrated from $t = t_i$, $z = z_i$ to $t = t$, $z = z$, to give

$$\ln\left[\frac{z_\infty - z_i}{z_\infty - z}\right] + \frac{z_i - z}{z_\infty} = \frac{k(t - t_i)}{z_\infty^2} \tag{8}$$

Substituting the appropriate values of I_i, I and I_∞ from Equation (1), one obtains

$$\ln\left[\frac{1 - \frac{I_\infty}{I_i}}{1 - \frac{I_\infty}{I}}\right] + \left[\frac{I_\infty}{I_i} - \frac{I_\infty}{I}\right] = \frac{f^2(t - t_i)}{k} \tag{9}$$

The initial time is often chosen to be as close as possible to the time at which the ECM voltage is applied to the electrode and tool feeding is commenced to ensure that the initial gap in these experiments can be approximated to that set before machining. In practice, this time is often the point at which the current stops its initial decrease, denoting the establishment of stable machining conditions. The values at this time (termed time zero) are given the subscript 0 in this paper to denote this.

For the planar segmented tool, Equation (9) should also apply to segments 2–6, with each of the segments having an identical electrode area, designated as $A = A_n$ and segment currents of $I_0 = I_{n,0}$ and $I_\infty = I_{n,\infty}$ in Equations (1), (2) and (6). Hence, each should give a similar current–time response to the planar single tool system. This is because the assumption of normal field lines between the workpiece and tool electrodes should largely apply to each of these segments, with the exception of the relatively thin intersegment insulating regions of the segmented tool. Since these insulating regions are small in area compared to the area of the segments (0.05 mm compared to 5.95 mm), they would therefore be expected to have a relatively small effect on the overall response. It is important to note that for segments 2–6, A_n corresponds to the area of one segment plus one intersegment insulating region, whilst for segments 1 and 7, A_n is the area of the segment plus half an insulating region, as this is the area of workpiece being eroded by each segment.

Figure 4 shows representative data for segments 2 and 6 for machining In718 with nitrate electrolyte, along with the iterative fits produced using Equation (9). Good fits to these data are obtained in all cases, from which values of f^2/k and $I_{n,\infty}$ (I_∞ for each segment, n) have been obtained. Furthermore, k/f^2 and $I_{n,0}$ data ($I_{n,0}$ being the initial current for segment n at the onset of machining) obtained for these fits can be compared to the values previously obtained using the planar single tool/planar workpiece configuration [6] (Figure 5). The single tool data showed that both k/f^2 and I_0 have a linear dependence with V, indicating approximately constant values of $V_0 = 5.4 \pm 0.4$ V, $\kappa = 0.20 \pm 0.010$ S cm^{-1} and $n = 3.0 \pm 0.2$ for the In718 system in nitrate electrolyte. The observed close correlation of the mean values of k/f^2 and I_0 for the segments at each value of V with those found from the previous single tool data demonstrates that ECM of In718 occurs with similar values of V_0, κ and n in both single and segmented tool experiments. Also, observed values of $I_{n,\infty}/A_n$ were found to be 72 ± 2 A cm^{-2} for all segments, in good agreement with I_∞/A values from the single tool experiments [6]. This confirms the applicability of the normal field line approximation to the segmented tool system and of Equation (9) to segmented tool data analysis for segments 2–6. This also validates the assumption of a constant efficiency for the dissolution reaction along the flow path length.

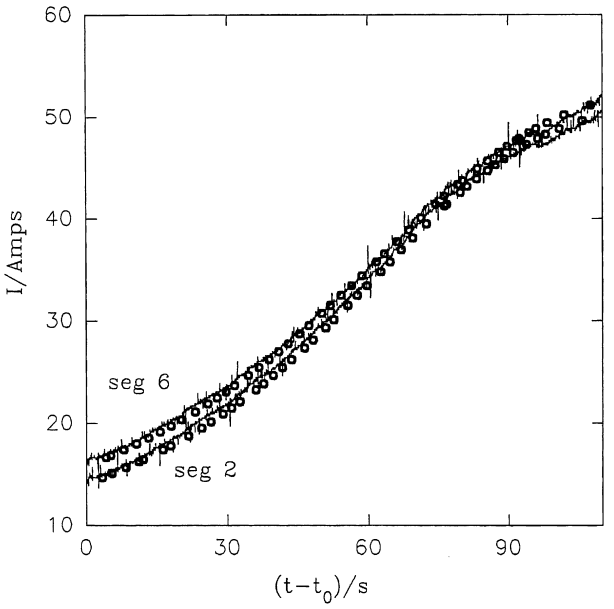

Fig. 4. Experimental current–time data (-) and theoretical fits to these data from Equation. (9) (o) for segments 2 and 6 for In718 in nitrate electrolyte at $V = 16$ V.

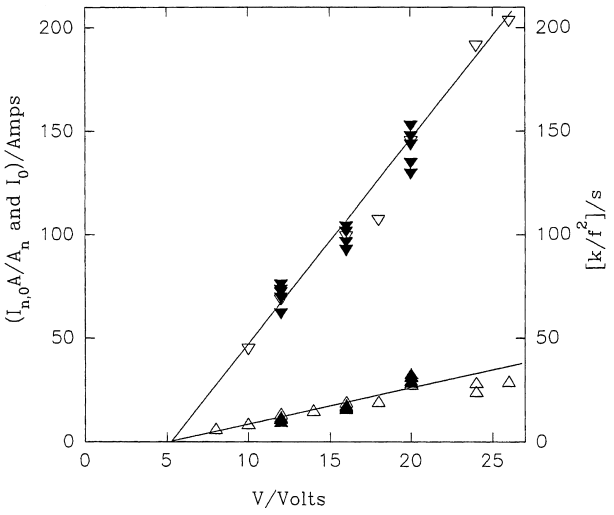

Fig. 5. Comparison of the values of $I_{n,0}$ and k/f^2 obtained for In718 in nitrate by the iterative fits to Equation (9) for each of segments 2–6 at $V = 12$, 16, 20 V (▼) with equivalent data (I_0 and k/f^2) obtained using the planar single tool (▽) from reference [6]. $I_{n,0}$ data have each been multiplied by A/A_n to account for the difference in area between the single tool and each segment of the segmented tool, allowing direct comparison with I_0 data. At each voltage the values of both $I_{n,0}$ and k/f^2 were observed to increase with segment number.

Notwithstanding this, on close examination of the data, there is a small but significant increase in the values of $I_{n,0}$ and k/f^2 with increasing segment number at each value of V. It should be emphasised that the increase observed with the segmented tool is sufficiently small to explain the previously observed reasonable fit of the overall current data for a single tool to a constant mean value of k [6] and to justify the assumption of a constant k across each segment. The total increase in k is of the order of 10% (independent of the applied voltage, V) between segments 2 and 6. This can be attributed either to a 10% increase in the conductivity, κ, and/or a 10% increase in the value of $(V - V_0)$, due to a decrease in V_0. A decrease in V_0 would be due to a change in the voltage required to drive the workpiece dissolution reaction, arising from a change in the nature of this reaction or in the reagent concentrations across the workpiece surface. Such a variation would be unlikely to produce the observed approximately linear increase in k observed with increasing segment number. Furthermore, this increase in $(V - V_0)$ would be expected to be sensitive to the magnitude of the applied voltage, V, leading to a dependence of the total increase of k on V, which is not observed. Thus the observed increase is not likely to be due to a significant change in V_0, but rather to an increase in κ. A small change in electrolyte composition and/or temperature is the most likely cause. Thus this system can be used to quantify small changes in k along the flow path length.

When considering segments 1 and 7, it is clear from Figure 3b that these tool segments overlap the workpiece, and that the migrational current will have a significant contribution from non-normal field lines. Initially, the migration can be modelled as two distinct areas. The first extends over a width r_a and depth l (which is the depth of all the segments) and is where segment and workpiece lie directly above one another and show normal field lines. The second area applies to the overlapping ends of the tool over a width r_b and depth l, and corresponds to field lines converging on the edge of the workpiece as shown. In this case, the current due to migration for segment 1 or 7, $I_{1,7}$, can be approximated as the sum of two terms (assuming a constant workpiece–tool distance of z throughout)

$$I_{1,7} = \frac{\kappa(V - V_0) l r_a}{z} + \kappa(V - V_0) l \int_0^{r_b} \frac{1}{\sqrt{r^2 + z^2}} \mathrm{d}r \quad (10)$$

where the segment width is equal to the sum of r_a and r_b. By making the substitution $r/y = \tan u$, one obtains

$$I_{1,7} = \frac{\kappa(V - V_0) l r_a}{z} + \kappa(V - V_0) l \int_0^{\tan^{-1}(r_b/y)} \sec u \, \mathrm{d}u \quad (11)$$

Integration gives

$$I_{1,7} = \frac{\kappa(V - V_0) l r_a}{z} + \kappa(V - V_0) l \times \left[\ln\left(\sec\left(\tan^{-1} \frac{r_b}{y} \right) + \frac{r_b}{y} \right) \right] = \frac{\kappa(V - V_0) l r_a}{z} + \kappa(V - V_0) l \left(\ln \frac{\sqrt{2r_b^2 + z^2}}{z} \right) \quad (12)$$

and since $l r_n = A_n$, the area of segment $n = 2$–6, where r_n is the width of any of the segments n, by substitution one obtains [6]

$$I_{1,7} = \frac{I_n}{r_n} \left[r_a + B \ln \left(\frac{\sqrt{2r_b^2 + B^2}}{B} \right) \right] \quad (13)$$

where

$$B = \frac{z_\infty I_{n,\infty}}{I_n} = \frac{\kappa(V - V_0) A_n}{I_n} \quad (14)$$

from Equation (1), since I_n and $I_{n,\infty}$ are the current and equilibrium current (as t approaches infinity) for any of the segments $n = 2$–6 and z_∞ is the equilibrium distance between tool and workpiece. This means that B can be determined at any time for any segment n from the current I_n and either the values of z_∞ and $I_{n,\infty}$ or the values of κ and V_0 and the area of the segment, A_n. This allows the calculation of $I_{1,7}$ at any time from Equation (13) using the calculated values of B and the measured values of r_a, r_b, r_n and I_n. However, $I_{1,7}$ corresponds to the current that would be observed whilst maintaining a planar workpiece geometry. This will only rigorously apply at the onset of machining, as at the workpiece ends the increased migrational flux from the overlapping tool will lead to increased machining and an increasingly pronounced workpiece curvature, which has actually been observed after machining. The curvature causes an increased workpiece end to tool distance, resulting in a machining current less than that calculated in Equation (13). At longer times, machining conditions approach equilibrium, where there is no further change in either the tool–workpiece separation or the segment currents with time. Under these conditions, as the amount of metal dissolved from the workpiece per unit area by each segment will be the same and will exactly balance the feed rate, the currents for segments 1 and 7, $I_{1,7}$ will simply be given by

$$I_{1,7} = \frac{I_n r_a}{r_n} \quad (15)$$

with the particular condition as $t \to \infty$ of

$$I_{1,7,\infty} = \frac{r_a}{r_n} I_{n,\infty} \quad (16)$$

where $I_{1,7,\infty}$ and $I_{n,\infty}$ are the equilibrium machining currents for segments 1 or 7 and a neighbouring

segment, n, respectively. Thus experimental current–time transients obtained for segments 1 and 7 should be described by Equation (13) at short times and Equation (15) at long times, with a monotonic transition between these currents at intermediate times. This is indeed the case for both I_1 and I_7 (Figures 6 and 7),

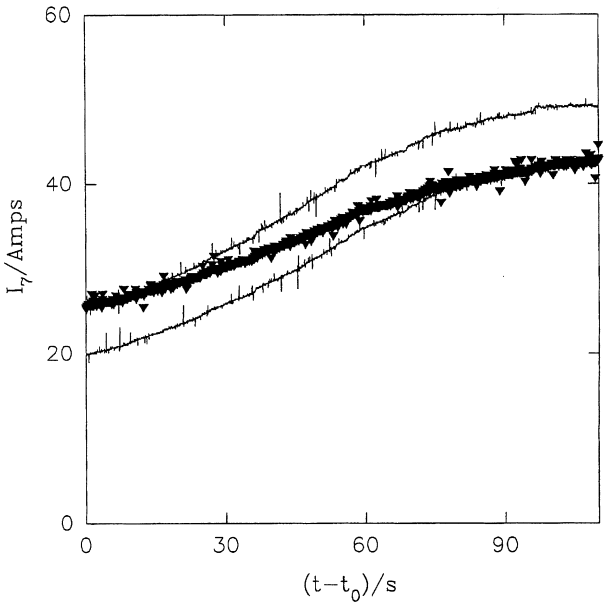

Fig. 6. Comparison of experimental current transient data for segment 7 (▼) measured at $V = 20$ V and an electrolyte flow rate of 16 dm^3 min^{-1} with theoretical data produced from Equation (13) (upper line) and Equation (15) (lower line) for ECM of In718 in nitrate electrolyte. Theoretical data for segment 7 have been calculated using Equation (13) and I_6 and z_∞ measured at segment 6.

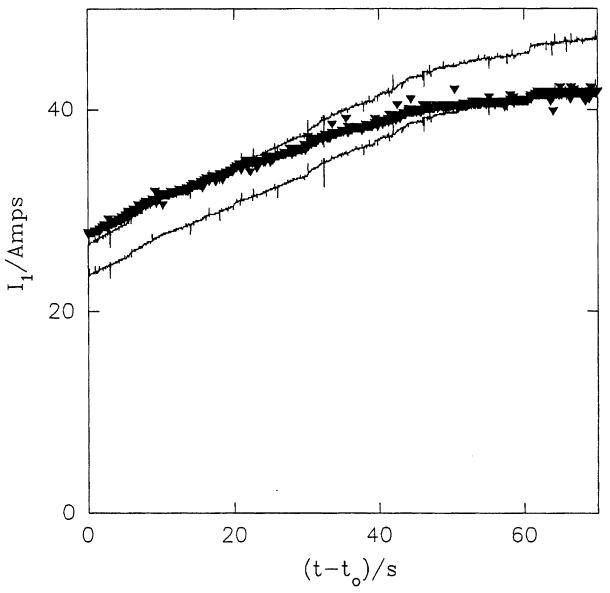

Fig. 7. Experimental current transient data for segment 1 (▼) measured at $V = 20$ V and an electrolyte flow rate of 22 dm^3 min^{-1} plotted against theoretical data produced from Equation (13) (upper line) and Equation (15) (lower line) for ECM of In718 in nitrate electrolyte. Theoretical data for segment 1 have been calculated using Equation (13) and I_2 and z_∞ measured at segment 2.

confirming the applicability of these models to these segments. I_1 can be seen to correlate closest with the currents predicted from segment 2 and I_7 with the currents predicted from segment 6, as the small differences in k observed on each segment necessitates comparison of neighbouring segments for the best correlation. This simple model does not incorporate any specific edge effects, as suggested by Landolt [20]. Thus, it is clear from the close correlation between theory and experiment that significant edge effects are not present in this system, and that correlation of experimental results obtained using the segmented tool system with theory could be used to probe these effects in other systems.

3.2. *ECM of SS316*

One application of the segmented tool is the measurement of changes in valency, such as those previously observed [24, 25] in the machining of stainless steel SS316 (En58J), where a smooth, bright surface was obtained at relatively high electrolyte flow rates and/or relatively low feed rates (low currents) and a dull, rough surface was produced at low flow rates and high currents (high feed rates). From consideration of the equilibrium erosion current and interelectrode gap, the bright surface was characterised as being due to Fe(III) and Cr(VI) dissolution and the dull surface to Fe(II) and Cr(III) dissolution. At intermediate flow rates, regions of shiny (upstream) and dull (downstream) surface were produced, with the proportion of shiny surface increasing with flow rate. This involved inspecting the workpieces after carrying out ECM for a fixed time at a variety of electrolyte flow rates [24]. Thus average valencies were produced and it was not possible to perform *in situ* measurements of the variation of this boundary position with time or to confirm the postulated variation of valency with flow path length. These spatially resolved and temporally resolved measurements have now been made using the segmented tool.

Figure 8 shows typical segmented tool current–time transients obtained from the ECM of SS316 under conditions analagous to fast flow rates, where a shiny surface finish was produced. As with In718 in nitrate electrolyte, similar current transients were observed for each segment, consistent with ECM occurring at a constant valency across the whole of the flow path length. Iterative fits to Equation (9) for each of the segments 2–6 produced a good fit to the experimental data, giving values of $I_{n,\infty} = 55 \pm 2$ A ($I_{n,\infty} = 75 \pm 3$ A cm^{-2}) in all cases. Since $M = 56.5$ g mol^{-1} and $\rho = 7.96$ g cm^{-3} for SS316, this gives a value of the valency from Equation (6) of $n = 3.0 \pm 0.1$ (assuming 100% efficiency of the machining process). This is consistent with the previous interpretation [24] of dissolution of the majority component as Fe(III) under these conditions. The values of k obtained both from I_0 and from k/f^2 produced by the iterative fits to Equation (9) were

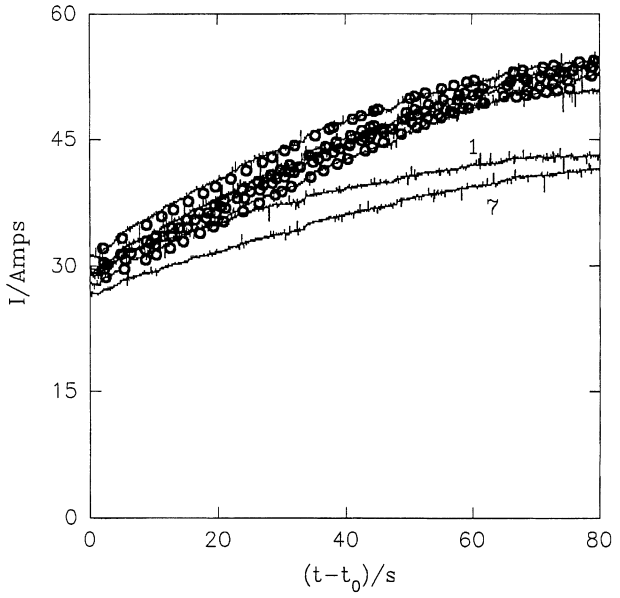

Fig. 8. Experimental current transient data (-) for segments 1–7 for ECM of SS316 at $V = 24$ V at an electrolyte flow rate of 22 dm^3 min^{-1}. Iterative fits to the current transient for segments 2–6 from Equation (9) are also shown (○). Segments 2–6 show a systematic decrease in I_0 with segment number. The transients for segments 1 and 7 are labelled.

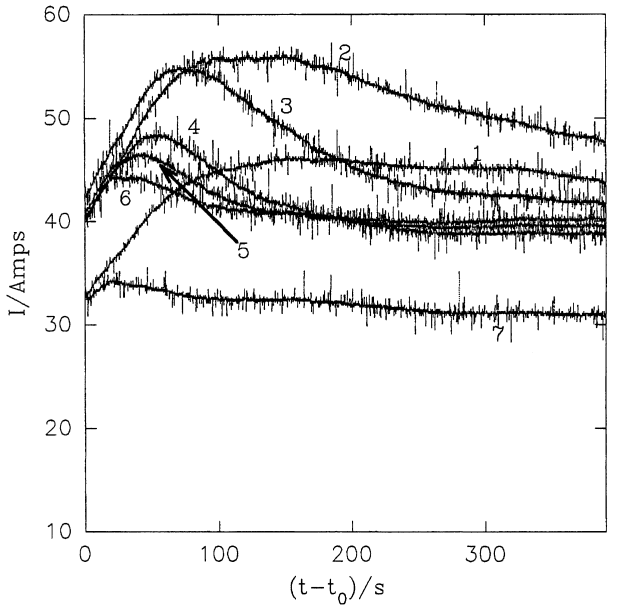

Fig. 9. Experimental current transient data (-) for segments 1–7 for ECM of SS316 at $V = 24$ V at an electrolyte flow rate of 16 dm^3 min^{-1}. The transient for each segment is labelled with the appropriate segment number.

observed to decrease by of the order of 10% from segments 2–6 (i.e. along the electrolyte path length), which is again sufficiently small to justify analysis with a constant κ for each segment. In contrast to the results for In718 in nitrate electrolyte, this is consistent with a small decrease in κ and/or an increase in V_0 along the electrolyte path length. For segments 1 and 7, $I_{n,\infty} = 44 \pm 1$ A, consistent with the calculated value from Equation (16) and $I_{n,\infty}$ of $I_{1,7,\infty} = 43 \pm 2$ A, which confirms that dissolution is occurring at the same valency across the whole of the workpiece surface. Substitution of the appropriate values of f^2/k, f, κ, ρ, V, M, n and F into Equation (5) gives a value of $V_0 = (12.4 \pm 0.5)$ V.

At slower flow rates, changes in valency are observed as expected (Figure 9). For $(t - t_0) \leqslant 150$ s, for segment 1, $I_{1,\infty}$=44 A and for segment 2, $I_{2,\infty}$= 57 A. This indicates that at equilibrium dissolution on these segments is occurring with $n = 3.0 \pm 0.1$ as before.

In contrast to segment 1, segment 7 shows very little change in ECM current with time, with $I_{7,\infty} = 31$ A. Since $I_\infty \propto n$ when comparing like segments, this corresponds to $n = 2.1 \pm 0.1$, entirely consistent with the previous interpretation of dissolution via Fe(II) downstream at low flow rates [24]. Furthermore, at times $(t - t_0) \geqslant 200$ s, a steady-state current of $I_{n,\infty} = 39 \pm 1$ A is established for segments 4–6, which also corresponds to $n = 2.1 \pm 0.1$, confirming that at these times for these segments dissolution occurs at this lower valency.

When comparing the current–time transients for segments 2–6, it is clear that there is a change in valency with time. Segment 2 shows a steady decrease in equilibrium current from $(t - t_0) \approx 160$ s onwards, attributable to a change in valency from $n = 3.0$ towards $n = 2.1$. Segments 3–6 show similar decreases, with significant deviation from the segment 2 transient at $(t - t_0) \approx 70$, 50, 35 and 25 s respectively. This deviation marks the progression of the 'boundary' between the areas machining at different valencies, which indicates that the boundary is moving upstream from segment 7 with time. Furthermore, the relatively slow decrease in each segment current with time indicates that the change in valency is not instantaneous, as does the observation that a decrease in valency is occurring on several segments simultaneously. Eventually, even the most upstream of segments is affected by this process, as evidenced by the observed decrease in current on segment 1 from $(t - t_0) \geqslant 300$ s. Further evidence for a gradual change has been acquired by terminating these experiments at different times and examining the workpiece surface. A clear correlation between the observed currents and the nature of the underlying workpiece surface was observed. Those segments with $n = 3.0$ had an underlying workpiece surface which was shiny, whilst for those with $n = 2.1$, the surface was dull. Those workpiece sections dissolving with $3.0 > n > 2.1$ had patches of shiny and dull surface, with the proportion of dull surface increasing as $n \to 2.1$. (However, even when the surface appeared completely dull, valencies above $n = 2.1$ could still be observed, indicating the presence of some areas of dissolution at increased valency). These observations therefore indicate that dissolution with a valency of $n = 2.1$ occurs initially on segment 7, producing a dull surface, and that this dull surface spreads progressively upstream across the workpiece surface with time, replacing dissolution with a valency of

$n = 3.0$, which is the cause of the shiny surface. These experiments show that, contrary to previous suggestions [24], this change in surface finish and overall dissolution valency occurs relatively slowly and simultaneously across several segments. We are presently investigating the chemistry of this dissolution process.

4. Conclusions

The results show that modification of a planar ECM system [6] to incorporate a segmented tool allows the variation of ECM parameters to be measured along the electrolyte flow path length. Variations in the electrolyte conductivity (κ, due to changes in electrolyte composition and/or temperature) and in the dissolution valency (n) have been measured, and the use of overlapping end segments has allowed edge effects (or throwing power effects) to be monitored. Such measurements are crucial to the parameterisation of the ECM of long flow-path length processes for industrial applications. Furthermore, these measurements can be made during machining, allowing both temporal and spatial changes to be monitored and giving insight into the time-dependent and current and voltage dependent electrochemical processes occurring which give rise to the ECM parameters observed.

Acknowledgements

We wish to thank EPSRC for support and for the provision of a studentship for PSH. We also gratefully acknowledge the support of Alan Cannon and Rolls-Royce plc and of Mike Yardley and Doncasters plc.

References

1. D.G. Risco and A.D. Davydov, *J. American Soc. Mech. Eng.* **64** (1993) 701.
2. M.A. ElDardery, *Int. J. Machine Tool Des. Res.* **22(3)** (1982) 147.
3. B. Kellock, *J. Machinery Product. Eng.* **140(3604)** (1982) 40.
4. O.V.K. Chetty and R.V. Murthy Radhakrishan, *Trans. of the ASME J. Eng. Ind.* **103(3)** (1981) 341.
5. A.R. Mileham, S.J. Harvey and K.J. Stout, *J. Wear* **109** (1986) 207.
6. A.R. Mount, K.L. Eley and D. Clifton, *J. Appl. Electrochem.* **30** (2000) 447.
7. A.K. Karimov, *J. Soviet Aeronautics* **28(3)** (1985) 105.
8. A.G. Makie, *J. Mathematical Anal. Apps.* **117(2)** (1986) 548.
9. J. Kozak, L. Dabrowski, K. Lubkowski and M. Rozenek, *Proc. 13th. Int. CAPE Conf.*, (Warsaw, 1997) p. 311.
10. H. Tipton, *Proc 5th Int. Confer. Adv. Machine Tool Des. Res.* (1964) 509.
11. A.D. Davydov and V.D. Kanshcheev, *Elektronnaya Obrabotka Materialov* (1985) 80.
12. H. Hardesty, A.R. Mileham and H. Shirrani, *Proc. Inst. Mech. Engrs.* **211B** (1997) 197.
13. O. Narayanan, S. Hinduja and C.F. Noble, *Int. J. Mach. Tool Des. Res.* **26** (1986) 323.
14. V.K. Jain and P.C. Pandey, *Precision Engr.* **2** (1980) 195.
15. G.M. Alder, D. Clifton and F. Mill, *Proc. Inst. Mech Engrs.* **214B** (2000) 745.
16. W.G. Clark and J.A. McGeough, *J. Appl. Electrochem.* **7** (1977) 277.
17. J. Hopenfield and R.R. Cole, *J. Eng. Ind.* **88** (1966) 455.
18. J. Hopenfield and R.R. Cole, *J. Eng. Ind.* **91** (1969) 755.
19. A.P. Shulepov, A.V. Kaptsov, V.A. Shmanev and V.G. Filimoshin, *Sov. Surf. Eng.* **5** (1987) 78.
20. D. Landolt, *J. Electrochem. Soc.* **119** (1972) 708.
21. M. Datta and D. Landolt, *Electrochim. Acta* **25** (1980) 1263.
22. D. Landolt, *J. Electrochem. Soc.* **119** (1972) 708.
23. M.A. Bejar and F. Gutierrez, *J. Mater. Processing Tech.* **37** (1993) 691.
24. P.J. Moir and S.J. Harvey, *Proc. of 16th Matador Conference* (1976) 275.
25. A.R. Mileham, R.M. Jones and S.J. Harvey, *Production Points, Precision Eng.* **4** (1982) 168.